

# Giant vortex state in perforated aluminum microsquares

V. Bruyndoncx\*, J. G. Rodrigo, T. Puig†, L. Van Look, V. V. Moshchalkov  
*Laboratorium voor Vaste-Stoffysica en Magnetisme,  
Katholieke Universiteit Leuven, Celestijnenlaan 200 D, B-3001 Leuven, Belgium*

R. Jonckheere  
*Interuniversity Micro-Electronics Center, Kapeldreef 75, B-3001 Leuven, Belgium*  
(October 19, 2018)

## Abstract

We investigate the nucleation of superconductivity in a uniform perpendicular magnetic field  $H$  in aluminum microsquares containing a few (2 and 4) submicron holes (antidots). The normal/superconducting phase boundary  $T_c(H)$  of these structures shows a quite different behavior in low and high fields. In the low magnetic field regime fluxoid quantization around each antidot leads to oscillations in  $T_c(H)$ , expected from the specific sample geometry, and reminiscent of the network behavior. In high magnetic fields, the  $T_c(H)$  boundaries of the perforated and a reference non-perforated microsquare reveal cusps at the same values of  $\Phi/\Phi_0$  (where  $\Phi$  is the applied flux threading the total square area and  $\Phi_0$  is the superconducting flux quantum), while the background on  $T_c(H)$  becomes quasi-linear, indicating that a giant vortex state is established. The influence of the actual geometries on  $T_c(H)$  is analyzed in the framework of the linearized Ginzburg-Landau theory.

72.25.Dw, 74.60.Ec, 73.23.-b

## I. INTRODUCTION

Recent experiments on mesoscopic superconducting aluminum structures with sizes smaller than the temperature dependent coherence length  $\xi(T)$  and penetration depth  $\lambda(T)$  have shown the influence of the sample topology on the superconducting critical parameters, like the normal/superconducting phase boundary  $T_c(H)$  (i.e. the critical temperature  $T_c$  in the presence of an applied magnetic field  $H$ )<sup>1</sup>. Many different topologies have been studied experimentally and theoretically.

First of all, there are structures made of quasi-one-dimensional strips, which can be further classified into single loops<sup>2-4</sup> (where  $T_c(H)$  shows the well-known periodic Little-Parks oscillations<sup>5</sup>), multiloop structures<sup>6-10</sup> (double loop, yin-yang, lasso, 2×2-cell, etc.) and large infinite networks<sup>11</sup>. The theories used to calculate the  $T_c(H)$  for these structures are based on the linearized Ginzburg-Landau theory, using either the de Gennes-Alexander formalism<sup>9</sup> or the London limit<sup>12,13</sup>. The fluxoid quantization constraint (i.e. the requirement that the order parameter is uniquely defined after integration of the phase gradient along a closed superconducting contour) in these 'multiply connected' structures gives rise to the oscillatory shape of the phase boundaries  $T_c(H)$ , superimposed usually on a parabolic background.

Secondly, surface superconductivity effects in (circular or square shaped) single dots<sup>1,14-16</sup> and antidots<sup>17-19</sup> (i.e. one antidot in a plain film) have been studied intensively. In these structures,  $T_c(H)$  consists of oscillations, which are pseudoperiodic. The appearance of the giant vortex state, where superconductivity is nucleated only near the sample boundary<sup>1,14,16,20-22</sup>, is due to the quantization of the phase winding number  $L$  of the superconducting order parameter  $\Psi = |\Psi| e^{-iL\varphi}$  (this is equivalent to fluxoid quantization). For cylindrically symmetric structures, one refers to  $L$  as the angular (or orbital) momentum quantum number<sup>3</sup>. For the states  $L > 1$ , the dot (or antidot) area is threaded by multiples  $L$  of the superconducting flux quantum  $\Phi_0 = h/2e$ . This "surface superconductivity" gives rise to a quasi-linear critical field  $H_{c3}$  versus temperature  $T$ , which we will further compare with the experimental  $T_c(H)$ .

The experimental studies of the antidot structure are usually carried out on samples with regular lattices of antidots. It was shown by Bezryadin *et al.* that, at sufficiently high magnetic fields, the antidots behave independently<sup>18</sup>. In these systems, the antidots create efficient pinning centers for the flux line lattice<sup>23</sup>.

We will present the measured phase boundaries  $T_c(H)$  of three different topologies, which are shown in Fig. 1. The three structures studied are a filled microsquare, and two squares with 2 and 4 square antidots respectively. Similar structures were studied in Refs.<sup>7,8</sup>, where the 4-antidot structure was proposed as a basic cell for a memory based on flux logic. In those papers, different stable vortex configurations were detected at low magnetic fields.

The goal of the present report is to study the influence of the antidots inside a microsquare on the crossover from the "network" behavior at low fields to a giant vortex state<sup>21,22</sup> at higher fields, and whether eventually the two configurations (vortices pinned by the antidots and the giant vortex state) can coexist. We will mainly focus on the high magnetic field regime. In a structure with one single antidot (i.e. a loop, as in Ref.<sup>1</sup>) as well, the presence of a giant vortex state can be anticipated at sufficiently high magnetic fields. In such a system, however, the phase winding number  $L$  will be identical for every contour encircling

the antidot. The development of the giant vortex state is accompanied by a transition from a parabolic background in  $T_c(H)$  to a quasi-linear  $T_c(H)$  behavior. The crossover field is strongly dependent on the size and the aspect ratio of the loop and will be the subject of a future paper. For the loop studied in Ref.<sup>1</sup>, the magnetic field was clearly not sufficiently high to reach this transition regime.

The advantage of a structure with more than one antidot is the property that each antidot can in principle contain a different number  $L$  of flux quanta  $\Phi_0$ . Simultaneously, a quantum number  $L$  is attributed to the outside square. The observed cusps in  $T_c(H)$  can then be related to the switching of either the quantum state of an antidot, or of the whole square.

For the 4-antidot structure, a 'collective' or network behavior can be expected at low magnetic fields<sup>7</sup>, while a 'single object' regime<sup>18</sup> can be reached at higher fields, where at  $T_c(H)$  a surface superconducting sheath develops near the sample boundary. The comparison of the  $T_c(H)$  data obtained on the perforated Al microstructures with that of a reference microsquare without antidots confirms the presence of a giant vortex state in the three structures in the high magnetic field regime.

## II. EXPERIMENT

Three different microstructures, shown in Fig. 1, have been studied. A square dot, with side  $a=2.04 \mu\text{m}$  is taken as a reference sample (a); a square of side  $a=2.04 \mu\text{m}$ , with four  $0.46 \times 0.46 \mu\text{m}^2$  square antidots (b); and a square, side  $a=2.14 \mu\text{m}$ , with two  $0.52 \times 0.52 \mu\text{m}^2$  antidots, placed along a diagonal (c). For the 4-antidot sample (b) the width of the superconducting outer stripes is  $0.33 \mu\text{m}$  and the inner stripes are  $0.46 \mu\text{m}$  wide. For the 2-antidot sample (c) the outer stripes are  $0.35 \mu\text{m}$  wide, and the non-perforated areas are  $1.27 \mu\text{m}$  wide. The dimensions are summarized in Table I. Electrical contacts have been attached to the samples using an ultrasonic wire bonding technique on the  $150 \times 150 \mu\text{m}^2$  large contact pads.

The three samples have been prepared in a single run by thermal evaporation of 99.999 % pure Al on a  $\text{SiO}_2$  substrate. The patterns are defined using e-beam lithography on a bilayer of PMMA resist previous to the deposition of a 24 nm thick aluminum film. After the evaporation, the liftoff was performed using dichloromethane. The structures were characterized by X-ray, SEM and AFM (Fig. 1).

Four-point resistance measurements were performed in a  $^4\text{He}$  cryostat, using a PAR 124A lock-in amplifier. A measuring current of 100 nA r.m.s. with a frequency of 27 Hz was used, which is depressing the  $T_c$  by only a few millikelvins, in the whole magnetic field range.

The  $T_c(H)$  measurements are done in a continuous run, keeping the sample resistance typically at 50 % of the normal state value and sweeping the magnetic field slowly while recording the temperature. The magnetic field was applied perpendicular to the structures, and a temperature stability better than 0.5 mK was achieved.

### III. RESULTS

In Fig. 2 we present the experimental phase boundary  $T_c(H)$  of the three structures. The measured  $T_c(H)$  values were independent of the direction of the magnetic field scans and were reproduced in several measurement rounds. In this paper we will always plot  $T_c(H)$  in the usual way, i.e. with the  $T_c$ -axis pointing from the highest to the lowest temperature. Peaks in the  $T_c(H)$  plots are then in reality local minima of the critical temperature  $T_c$ .

For the reference full square, we observe pseudoperiodic oscillations in  $T_c(H)$  superimposed with an almost linear background, where the period of the oscillations slightly decreases with increasing field, in agreement with previous studies<sup>1,14,15,20,24</sup>. *These observations are characteristic for the presence of the giant vortex state.* For the perforated microstructures, *two different magnetic field regimes* can be distinguished. At *high magnetic fields*, the oscillations in  $T_c(H)$  are pseudoperiodic, just as the  $T_c(H)$  of the full square. For the *low field* part of the phase diagram, distinct features appear (i.e., below  $\sim 2.5$  mT): for the 2-antidot sample we observe the same number of peaks compared to the full square, but with a considerable shift of the positions of the first peaks. Compared to the full square  $T_c(H)$ , a new series of peaks, positioned symmetrically with respect to  $\mu_0 H \approx 1.4$  mT, is found for the 4-antidot sample, as can be expected for a  $2 \times 2$  cell network.

In what follows, we will investigate in detail the shape of  $T_c(H)$  in the two flux regimes for the three structures. We will discuss our results in terms of the existing models, within the Ginzburg-Landau (GL) theory, developed for mesoscopic structures with a cylindrical symmetry (disks, loops) which have been successfully applied earlier to interpret the results obtained in mesoscopic square structures<sup>1</sup>.

### IV. DISCUSSION

#### A. The $T_c(H)$ phase boundary of the full microsquare

The  $T_c(H)$  curve measured for the full square structure is very similar to the result obtained from a calculation<sup>16,20,22,24</sup> for a mesoscopic disk in the presence of a magnetic field (indicated as ' $H_{c3}$ ' in Fig. 2a). In that model the linearized first GL equation is solved with the boundary condition for an ideal superconductor/insulator interface:

$$\left(-i\hbar\vec{\nabla} - 2e\vec{A}\right)\Psi\Big|_{\perp,b} = 0, \quad (1)$$

which is the condition that no supercurrent can flow perpendicular to the interface. In the linear approach, the vector potential  $\vec{A}$  is related to the applied magnetic field  $\vec{H}$  through  $\mu_0\vec{H} = \text{rot}\vec{A}$ . In order to obtain the solutions which fulfill the boundary condition (Eq. (1)), one has to solve the equation:

$$(L - \Phi/\Phi_0) M(-n, L + 1, \Phi/\Phi_0) - \frac{2n\Phi/\Phi_0}{L + 1} M(-n + 1, L + 2, \Phi/\Phi_0) = 0 \quad (2)$$

The function  $M$  is the so-called Kummer function of the first kind,  $n$  is a real number depending on the phase winding number  $L$ , which has to be obtained numerically by solving

Eq. (2). The flux is defined as  $\Phi = \mu_0 H \pi R^2$ ,  $R$  being the radius of the disk. The  $T_c(\Phi)$  is obtained via the relation:

$$1 - \frac{T_c(\Phi)}{T_c(0)} = 4 \left( n + \frac{1}{2} \right) \frac{\xi^2(0)}{R^2} \frac{\Phi}{\Phi_0} \quad (3)$$

The upper critical field  $H_{c2}$  for a bulk superconductor is obtained when substituting  $n = 0$  in Eq. (3), which gives a linear relation between  $H_{c2}$  and  $T$ . However, for a finite size superconductor, a third critical field  $H_{c3}$  can be found, because the ground state is obtained from solutions of Eq. (2) with  $n < 0$ . Superconductivity is concentrated near the sample edge (for  $L > 0$ ), while the "normal" core contains one or several flux quanta  $L \Phi_0$ . This quasi-linear critical field  $H_{c3}(T)$  is the analog of the surface critical field for a semi-infinite superconducting slab in contact with vacuum (or insulator), where superconductivity persists in a surface sheath up to magnetic fields  $H_{c3}(T) \approx 1.69 H_{c2}(T)$  above the upper critical field<sup>25</sup>.

The series of peaks in the  $T_c(H)$  curve correspond to transitions between states with different angular momenta  $L \rightarrow L + 1$  of the superconducting order parameter as successive flux quanta,  $\Phi = L \Phi_0$ , enter the superconductor. A comparison with the experimental result for a square structure was made in Ref.<sup>1</sup>. In a very recent paper by Jadallah *et al.*<sup>26</sup> the  $T_c(H)$  phase boundary is studied theoretically and is compared to the experimental  $T_c(H)$  curve for the full square, described in the present paper.

Following Ref.<sup>14</sup>, between  $\Phi=0$  and the first peak located at  $\Phi = 1.92 \Phi_0$ , the superconducting order parameter  $\Psi$  has angular momentum  $L = 0$ , and the reduced critical temperature is quadratic in  $\Phi$ :

$$1 - \frac{T_c(\Phi)}{T_c(0)} = \frac{\xi^2(0)}{2R^2} \left( \frac{\Phi}{\Phi_0} \right)^2 \quad (4)$$

The quasi-linear background at high flux,  $\Phi/\Phi_0 \gg 1$ , follows the asymptotic expression:

$$1 - \frac{T_c(\Phi)}{T_c(0)} = \frac{2}{\eta} \frac{\xi^2(0)}{R^2} \frac{\Phi}{\Phi_0} \quad (5)$$

The parameter  $\eta$  represents the ratio of the ground state energy ( $H_{c3}$ ) to the lowest bulk Landau level ( $H_{c2}$ ) and therefore coincides with the ratio  $H_{c3}/H_{c2}$  at a fixed temperature. For  $\Phi/\Phi_0 \rightarrow \infty$ , in other words for  $R \rightarrow \infty$ , the value  $\eta \rightarrow 1.69$ . Note that substituting  $\eta = 1$  in Eq. (5) gives the equation for  $H_{c2}(T)$  (or  $T_{c2}(H)$ ), indicated by the straight line labeled ' $H_{c2}$ ' in Fig. 2a.

When matching the position of the experimental and theoretical peaks, we obtain a value for the field corresponding to one flux quantum,  $\mu_0 H_0 = 0.53$  mT. This scaling leads to a very good agreement in the position of all the peaks (see the inset of Fig. 3) and strongly supports the validity of applying this model to our experiments. From  $H_0$  we obtain an effective area of  $3.9 \mu m^2$ , close to the actual size of the structure,  $4.2 \mu m^2$ . The introduction of this 'effective area' is obviously not needed if the  $T_c(H)$  is compared with a calculation performed for a square<sup>26</sup>. Then, from Eq. (4), we find the coherence length,  $\xi(0)=92$  nm (dashed line in Fig. 2a), and using the values for pure Al and the Ginzburg-Landau expressions for *dirty* superconductors<sup>27</sup>, we can estimate the mean free path,  $\ell=7$  nm, and the penetration

depth,  $\lambda(0)=140$  nm. The results for the three structures are summarized in Table I. The determined value  $\xi(0)=92$  nm might be a bit too low, since at low magnetic fields the electrical leads attached to the square can give rise to nonlocal effects<sup>28</sup>. Simultaneously, fitting the low field part of the experimental  $T_c(H)$  to Eq. (6) of Ref.<sup>26</sup> gives an increased  $\xi(0)=95$  nm.

In contrast to the experimental result presented in Ref.<sup>14</sup>, which was obtained for a substantially larger, but circular dot, the field period can be matched to the theoretical predictions in the whole field interval. The distance  $\Delta\Phi$  between the peaks in  $T_c(\Phi)$  follows the asymptotic limit  $\Delta\Phi = \Phi_0 \left(1 + (2\eta\Phi/\Phi_0)^{-1/2}\right)$ . In our experiment  $\Delta\Phi$  reaches a nearly constant value for  $\Phi/\Phi_0 \geq 6$ , with  $\mu_0 \Delta H \simeq 0.60 - 0.65$  mT. When a sufficiently high magnetic field is applied to the sample, a superconducting edge state is formed, where superconductivity only nucleates within a surface layer of thickness  $w_H = \sqrt{\Phi_0/2\eta\pi\mu_0 H}$ . The remaining area acts like a normal core of radius  $R_{\text{eff}} \approx R - w_H$ , and carries  $L$  flux quanta in its interior. Due to the expanding normal core, the sample can be seen topologically as a loop of variable radius. For this reason, the  $T_c(H)$  of the dot shows Little-Parks-like oscillations, which are, however, nonperiodic. The magnetic period  $\Delta H$  decreases, since the 'effective' radius grows with increasing field. In contrast to the case of the loop, which has a parabolic background on  $T_c(H)$ , the background is quasi-linear, because of the additional energy cost (i.e. extra reduction of  $T_c$ ) for depressing superconductivity in the sample core. As the applied magnetic field grows this 'giant vortex' core expands until it almost fills the entire sample area. According to this expression, at  $\mu_0 H=5$  mT, for example,  $w_H \approx 0.2 \mu\text{m}$  and the effective area of the normal core for the full square structure is  $\sim 3.3 \mu\text{m}^2$ . This value is in agreement with the observed magnetic period  $\mu_0 \Delta H$ .

The amplitude of the experimental oscillations is higher than expected from the theory (which was observed also in Ref.<sup>14</sup>) (see Fig. 2a). We carried out a few  $T_c(H)$  measurements, where we fixed the electronic feedback circuit at a different resistance value (10 – 90% of the normal state resistance  $R_n$ ). When a higher fixed resistance value was chosen (90% of  $R_n$ ), the amplitude of the  $T_c(H)$  oscillations was decreased. We should mention here that the measured resistance versus temperature curves, as the magnetic field increases, reveal a 'bump' above the normal state resistance, together with a significant broadening of the temperature interval in which the transition takes place. In Ref.<sup>29</sup> the bump was shown to appear in the 'superconducting state'. Since this disturbance is still small at low fields, we believe that the determination of  $\xi(0)$  from the low field formula (Eq. (4)) is rather accurate and therefore we use  $\xi(0)=92$  nm further on in this paper. The resistance peaks are caused by the electrical leads attached to the square, which have a higher transition temperature. For this reason, normal/superconducting boundaries are created at  $T \approx T_c$ , which, as in the experiment of Park *et al.*<sup>30</sup>, can give rise to a resistive transition showing a peak.

## B. The $T_c(H)$ phase boundaries of the perforated microsquares

Now, we will analyze the phase boundary observed for the 4-antidot structure (Fig. 2b). It shows similarities with the full square: there is a quasi-linear background with pseudoperiodic oscillations at high fields and the  $T_c(H)$  is parabolic for low magnetic fields (dashed line in Fig. 2b). At the same time new features (extra peaks) are clearly seen below  $\sim 2.5$  mT.

Let us first discuss the  $T_c(H)$  curve in this low field regime. We will compare it with the  $T_c(H)$  calculated for a  $2 \times 2$ -cell network consisting of one-dimensional strips. Strictly speaking, the theory for networks is valid only when the width of the strips forming the structure are much smaller than  $\xi(T)$ . For the dimensions of the sample studied here, variations of  $\Psi$  along the strip width can be expected if  $T$  is slightly below  $T_c(0)$ . The de Gennes-Alexander (dGA) model<sup>9</sup>, based on the linearized Ginzburg-Landau equations, has been used successfully to explain the phase boundaries obtained in mesoscopic single- and multiloop structures<sup>1,6</sup> with narrow superconducting strips. The depression of  $T_c(H)$  can be expressed as the sum of a topology dependent oscillatory component and a parabolic term (dashed line in Fig. 2b) which is due to the finite width  $w$  of the strips:

$$1 - \frac{T_c(H)}{T_c(0)} = \frac{\pi^2}{3} \left( \frac{w\xi(0)\mu_0 H}{\Phi_0} \right)^2 \quad (6)$$

In Fig. 4 we compare the low magnetic field part of the experimental  $T_c(H)$ , where a parabolic background (Eq. (6)) with an averaged (over inner and outer strips) width of  $0.4 \mu m$  has been subtracted, with the  $T_c(H)$  obtained from the dGA model. In Ref.<sup>10</sup> (Eqs. 20-22) and Ref.<sup>8</sup> (Eq. 3.12) the functions forming the  $T_c(H)$  for a  $2 \times 2$ -cell network can be found. The field corresponding to one flux quantum per elementary cell is 2.8 mT, leading to an effective total area for the  $2 \times 2$ -cell network of  $2.96 \mu m^2$  ( $0.74 \mu m^2$  per cell, the side length of each cell  $a=0.86 \mu m$ ). The theoretical  $T_c(H)$  reproduce the observed flux (or fluxoid) states, and have been calculated with  $\xi(0)=92$  nm (dashed line in Fig. 4), obtained for the full square, and with  $\xi(0)=140$  nm (solid line in Fig. 4), estimated from the parabolic background (Eq. (6)).

It is clear that, for increasing magnetic field, the  $T_c(H)$  of the 4-antidot structure can no longer be calculated from the dGA model, since  $\xi(T)$  becomes comparable to the width of the strips, giving rise to spatial variation of  $\Psi$  perpendicular to the strips.

Let us point out the differences between the  $T_c(H)$  of the present 4-antidot structure and the previously measured '2x2-antidot cluster' made of Pb/Cu<sup>7,8</sup>. In the present Al structure, the network features are not periodically repeated as the magnetic field is increased. Instead, above 2.8 mT, the positions of the successive peaks coincide with the peaks observed in the  $T_c(H)$  of the reference full square. Moreover, the background clearly starts deviating from parabolic to quasi-linear. Contrary to this, in the Pb/Cu antidot cluster (see Fig. 1 in Ref.<sup>7</sup>) the peaks related to the network behavior are visible over two periods, i.e. up to  $\mu_0 H \approx 5$  mT. For higher fields, no giant vortex state can be deduced for the Pb/Cu sample, since the background reduction of  $T_c$  stays parabolic and  $T_c(H)$  shows pronounced peaks instead of cusps.

The main parameter which determines the  $T_c(H)$  is the coherence length  $\xi(T)$ . Since the coherence length  $\xi(0)$  of Al is approximately three times larger than for Pb/Cu, the relative  $T_c$  reduction  $\delta T_c = 1 - T_c(H) / T_c(0)$  is almost a factor 10 higher in Al than in an identical Pb/Cu sample (see Eqs. (3)-(6)). Since, for a particular sample geometry,  $\delta T_c / \xi^2(0) = 1 / \xi^2(T)$  should only depend on the magnetic field (at  $T = T_c(H)$ ), the penetration depth  $\lambda(T)$  might play an important role. Using  $\lambda^2(T) = \lambda^2(0) / \delta T_c$ , with  $\lambda(0)=140$  nm for Al, and  $\lambda(0)=76$  nm for Pb/Cu<sup>7,8</sup>, we obtain  $\lambda(T = T_c^{Al}) \approx 0.6 \lambda(T = T_c^{Pb/Cu})$ . In other words, the assumption  $\mu_0 \vec{H} = rot \vec{A}$  (corresponding to  $\lambda \gg w$ ) is fulfilled up to higher magnetic fields in the case of Pb/Cu. This is consistent with the fact that, the peaks due to

switching of the state of single antidots, is seen up to higher fields in Pb/Cu, but it does not explain the very different behavior in the two materials of course. Other possibilities might be related to the proximity effect in Pb/Cu, as well as to a different saturation number<sup>31</sup>  $n_s \approx R/(2\xi(T))$  in the two materials, although the simple formula for  $n_s$  was obtained only for a single antidot surrounded by a large superconducting area and might not be valid here.

For the (slightly larger) 2-antidot Al structure (Fig. 2c) the interpretation of the low field regime of  $T_c(H)$  is more difficult. We will return briefly to this point later in the paper. At high fields, however, the positions of the peaks in  $T_c(H)$  correspond to the same pseudoperiodic oscillations as for the full square and 4-antidot structure.

In Fig. 3 we have replotted the phase diagram in units of  $\Phi/\Phi_0$ . It is important to note that we defined the flux as  $\Phi = \mu_0 H S_{eff}$ , with  $S_{eff}$  the effective area of the whole microsquares. It is close to the exact outer sample area  $S$ , and was introduced in order to fit the peak positions to the calculated  $T_c(\Phi)$  for a circular dot. To avoid confusion, we want to mention the different definition of flux in Refs.<sup>7,8</sup> (antidot cluster), where flux is referred to the area available for one single antidot. In the case of a loop<sup>1,28</sup>, it is natural to define the flux as the area enclosed by a contour through the middle of the strips multiplied by the magnetic field, in order to ensure a perfectly periodic  $T_c(\Phi)$ , with a period  $\Phi_0$ .

Since the 2-antidot structure is a bit larger than the two other structures, a different  $H_0$  is used to scale the magnetic field. In the inset the positions of the peaks in the experimental  $T_c(\Phi)$  are compared with the theoretical prediction for a mesoscopic superconducting disk. The  $n$ -th peak corresponds to the transition between the state  $L = n - 1$  and  $L = n$  (for the 4-antidot sample the peak numbers have been reassigned due to the extra peaks in the network regime). At high magnetic fields, there is a quite good agreement of the peak positions of the three structures and a good correspondence with the theoretical values found for the disk, which is drawn in the inset of Fig. 3 as a solid line.

How can we understand this striking coincidence of the peak positions at high fields for the three structures? For this, we have to look how the superconducting order parameter nucleates along a curved superconductor/insulator boundary. Figure 5a shows the calculated  $T_c(\Phi)$  curves for a single circular dot and for an antidot (see also Ref.<sup>18</sup>) in an infinite film, both of radius  $R$ . The latter has been calculated in a similar way as the  $T_c(\Phi)$  of the dot. For a single antidot, the boundary condition (Eq. (1)) translates into:

$$(L - \Phi/\Phi_0)U(-n, L + 1, \Phi/\Phi_0) + 2n \frac{\Phi}{\Phi_0} U(-n + 1, L + 2, \Phi/\Phi_0) = 0, \quad (7)$$

where the function  $U$  is the Kummer function of the second kind, diverging at the origin, i.e. at the center of the antidot. The numeric values for  $n$  have to be inserted into Eq. (3), to obtain the  $T_c(\Phi)$ .

In Figure 5b the respective enhancement factors  $\eta$  (corresponding to  $H_{c3}/H_{c2}$ ) are shown. For both the dot and the antidot the value  $\eta=1.69$  is approached as the curvature radius  $R$  goes to infinity (or for a fixed  $R$ , as  $H \rightarrow \infty$ ). Since the dot has a larger  $\eta$  than the antidot, corresponding to a higher  $H_{c3}(T)$ , the superconducting order parameter is expected to grow initially at the outer sample boundary, as the temperature drops below  $T_c$ . At slightly lower temperatures surface superconductivity should as well nucleate around the antidots. In the mean time, however, the order parameter has reached already a finite value over the whole width of the strips. In the complete temperature (or flux) interval of our



measurements  $\eta < 1.5$  for the antidots and  $\eta > 1.8$  for the dot (when scaling the radii to the actual sample dimensions). The resistively measured phase transitions, probably because of this substantially different  $H_{c3}$  for a dot and an antidot, only show peaks related to the switching of the angular momentum  $L$ , associated with a closed contour along the outer sample boundary. At the  $T_c(H)$  boundary, in the high magnetic field regime, there is no such closed superconducting path around each single antidot, and therefore the fluxoid quantization condition does not need to be fulfilled for a closed contour encircling each single antidot.

Although a more detailed analysis has to be carried out, since the sample boundaries in our experiments have sharp corners, the interpretation given above is expected still to be valid. A detailed analysis of a square *loop* geometry performed by Fomin *et al.*<sup>32</sup> has shown that the superconducting order parameter preferentially nucleates near the sharp corners of the structure. In another paper, the same authors discuss the enhancement of the surface critical field  $H_{c3}$  above the bulk upper critical field  $H_{c2}$  in a semiplane, which is bent over a certain angle  $\alpha$  (superconducting wedge)<sup>33</sup>. The magnetic field is parallel to the wedge edge. An enhanced  $\eta$  value is found for angles  $\alpha < \pi$ , which can be as high as  $\eta = 3.79$  for  $\alpha = 0.44\pi$ . For angles  $\alpha > \pi$ , the surface critical field is not enhanced above  $\eta = 1.69$ . Note that the value  $\eta = 3.67$ , obtained for  $\alpha = \pi/2$  differs from the calculation in Ref.<sup>26</sup>, where for a square domain in the limit  $\Phi/\Phi_0 \rightarrow \infty$  the factor  $\eta \approx 1.8$  only. The discrepancy between these two results still has to be clarified.

For the 2-antidot structure, further quantitative calculations are needed to describe the low field behavior. Since there are no extra peaks present in  $T_c(\Phi)$ , compared to the full square, we believe that, here as well, a surface superconducting sheath develops along the outer sample boundary. At the lowest fields, the sheath width  $w_H$  is still larger than the width  $w$  of the strips, and therefore the position of the first peaks (mainly the second) in  $T_c(\Phi)$  are different from the full square.

In Fig. 6 the superconducting order parameter profiles are shown for a disk, calculated at different points  $\Phi/\Phi_0 = 1, 3, \dots, 17$  on the  $T_c(\Phi)$  curve. For  $\Phi/\Phi_0 = 1$  the ground state corresponds to  $L = 0$ , and the order parameter is only weakly modulated since there are no flux lines threading the sample. As we move to higher  $\Phi/\Phi_0$  superconductivity becomes more and more concentrated near the sample boundary. The presence of the antidots in the perforated samples produces different profiles for the superconducting order parameter, since the  $\Psi$  has to fulfill the boundary conditions (Eq. (1)) also at the antidot boundaries. A two-dimensional GL calculation would be required to obtain the proper order parameter distribution here.

The inset of Fig. 6 shows the width  $w_H$  of the edge state as a function of  $\Phi/\Phi_0$ . For our samples  $w_H$  becomes equal to the width of the strips at  $\sim (3 - 4)\Phi/\Phi_0$ . For fluxes above this value the presence of the antidots will not influence the position of the peaks in  $T_c(\Phi)$ . Therefore, at high fields, when  $w_H$  is smaller than the width of the outer strips in our structures, the order parameter is restricted to the outer border of the sample, and therefore it is impossible to have supercurrents around a single antidot.

The background depression of  $T_c$  is different for the three structures studied (Fig. 3). The larger the perforated area (in other words the smaller the area exposed to the perpendicular magnetic field), the less  $T_c(\Phi)$  is pushed to lower temperatures. Another clear example of a similar behavior is given in Ref.<sup>1</sup>, where the  $T_c(H)$  of the (square) dot is shown to be

lower than the  $T_c(H)$  of a the loop, when exposed to a perpendicular magnetic field. This general rule applies, for instance, also to simple strips for which  $T_c(H)$  is suppressed more when the width  $w$  increases, which is described by Eq. (6). In the dot of Ref.<sup>1</sup>, the giant vortex state was shown to develop. For the loop studied in that paper<sup>1</sup>, however, the used magnetic fields were too low to induce the crossover to a giant vortex state, which contrasts the observations from the present paper, in the high magnetic field regime.

The appearance of the giant vortex state in the high field regime is the most plausible explanation at the moment. We can not exclude, however, that another scenario is also possible. Namely, a nearly flat non-zero distribution of  $|\Psi|$  in the sample interior could coexist with an enhanced  $|\Psi|$  at the external sample boundary, although we believe that such a situation would give rise to peaks in  $T_c(\Phi)$  each time an antidot changes its quantum state. In any case, the final description of the specific shape of the superconducting order parameter at  $T_c(\Phi)$  requires a numerical two-dimensional calculation of  $\Psi$  for the perforated topologies, where the boundary conditions are fulfilled both at the outer and at antidot superconducting/insulator interfaces.

In summary, we have presented the experimental superconducting/normal phase boundaries  $T_c(H)$  of a mesoscopic full square and two perforated mesoscopic aluminum squares. The flux interval was divided in two regimes by comparing the results with the behavior of a full square microstructure: for low magnetic fields the 4-antidot structure behaves like a network consisting of quasi-one-dimensional strips, giving rise to extra peaks in  $T_c(H)$  in comparison to the full square. In the 2-antidot structure the peak positions are only shifted compared to the full square. As soon as each antidot contains one flux quantum, the giant vortex develops, resulting in pseudoperiodic oscillations in the  $T_c(H)$  and a quasi-linear background on  $T_c(H)$  at high magnetic fields. In this regime, the peak positions coincide for all three structures studied when the phase boundaries are plotted in flux quanta units (where flux is referred to the total sample area). For high magnetic fields, the presence of the antidots apparently does not change the phase winding number  $L$  for a closed contour around the outer perimeter of the whole square. Since the enhancement factor  $H_{c3}/H_{c2}$  is the highest at the outer sample boundary, superconductivity nucleates initially near the outside sample edges, resulting in a giant vortex state.

*Note added in proof:* The discrepancy between the result obtained by the authors of Ref.<sup>26</sup> and of Ref.<sup>33</sup> has been clarified in an erratum<sup>34</sup>.

## ACKNOWLEDGMENTS

The authors are thankful to the FWO-Vlaanderen, the Flemish Concerted Action (GOA) and the Belgian Inter-University Attraction Poles (IUAP) for the financial support. T. Puig wishes to thank the Training and Mobility of Researchers Program of the European Union. J. G. Rodrigo is a Research Fellow of the K.U.Leuven Onderzoeksraad. Discussions with Y. Bruynseraede, V.M. Fomin, J. Devreese, J. Rubinstein, C. Strunk and E. Rosseel are gratefully acknowledged.

\* e-mail: Vital.Bruyndoncx@fys.kuleuven.ac.be

† Present address: Institut de Ciencia de Materials de Barcelona - CSIC, Campus de la UAB, 08193 Bellaterra, Spain.

## REFERENCES

- <sup>1</sup> V.V. Moshchalkov, L. Gielen, C. Strunk, R. Jonckheere, X. Qiu, C. Van Haesendonck and Y. Bruynseraede, *Nature* **373**, 319 (1995).
- <sup>2</sup> H. Vloeberghs, V.V. Moshchalkov, C. Van Haesendonck, R. Jonckheere and Y. Bruynseraede, *Phys. Rev. Lett.* **69**, 1268 (1992).
- <sup>3</sup> M. Daumens, C. Meyers and A. Buzdin, *Physics Letters A* **248**, 445 (1998).
- <sup>4</sup> J. Berger and J. Rubinstein, cond-mat/9711043, scheduled for *Phys. Rev B* **59**, no 13, 1 april 1999.
- <sup>5</sup> W.A. Little and R.D. Parks, *Phys. Rev. Lett.* **9**, 9 (1962); R.D. Parks and W.A. Little, *Phys. Rev.* **133**, A97 (1964).
- <sup>6</sup> V. Bruyndoncx, C. Strunk, V.V. Moshchalkov, C. Van Haesendonck and Y. Bruynseraede, *Europhys. Lett.* **36**, 449 (1996).
- <sup>7</sup> T. Puig, E. Rosseel, M. Baert, M.J. Van Bael, V.V. Moshchalkov and Y. Bruynseraede, *Appl. Phys. Lett.* **70**, 3155 (1997).
- <sup>8</sup> T. Puig, E. Rosseel, L. Van Look, M.J. Van Bael, V.V. Moshchalkov, Y. Bruynseraede and R. Jonckheere, *Phys. Rev. B* **58**, 5744 (1998).
- <sup>9</sup> P.G. de Gennes, *C.R. Acad. Sci. Ser. II* **292**, 279 (1981); S. Alexander, *Phys. Rev. B* **27**, 2820 (1983); H.J. Fink, A. López and R. Maynard, *Phys. Rev. B* **26**, 5237 (1982).
- <sup>10</sup> R. Rammal, T.C. Lubensky and G. Toulouse, *Phys. Rev. B* **27**, 2820 (1983).
- <sup>11</sup> B. Pannetier, in *Quantum coherence in mesoscopic systems*, edited by B. Kramer, (Plenum Press, New York, 1991) and references therein.
- <sup>12</sup> S. Alexander, and E. Halevi, *J. Phys. (Paris)* **44**, 805 (1983).
- <sup>13</sup> C. C. Chi, P. Santhanam, and P. E. Blöchl, *J. Low Temp. Phys.* **88**, 163 (1992).
- <sup>14</sup> O. Buisson, P. Gandit, R. Rammal, Y.Y. Wang and B. Pannetier, *Phys. Lett. A* **150**, 36 (1990).
- <sup>15</sup> A. K. Geim, I. V. Grigorieva, S. V. Dubonos, J. G. S. Lok, J. C. Maan, A. E. Filippov, and F. M. Peeters, *Nature* **390**, 259 (1997).
- <sup>16</sup> V. A. Schweigert, F. M. Peeters, and P. S. Deo, *Phys. Rev. Lett.* **81**, 2783 (1998).
- <sup>17</sup> A. Bezryadin, A. Buzdin and B. Pannetier, *Phys. Rev. B* **51**, 3718 (1995).
- <sup>18</sup> A. Bezryadin and B. Pannetier, *J. Low Temp. Phys.* **98**, 251 (1995).
- <sup>19</sup> E. Rosseel, T. Puig, M. Baert, M.J. Van Bael, V.V. Moshchalkov and Y. Bruynseraede, *Physica C* **282-287**, 1567 (1997).
- <sup>20</sup> D. Saint-James, *Phys. Lett.* **15**, 13 (1965).
- <sup>21</sup> H.J. Fink and A.G. Presson, *Phys. Rev.* **151**, 219 (1966).
- <sup>22</sup> V.V. Moshchalkov, X.G. Qiu and V. Bruyndoncx, *Phys. Rev. B* **55**, 11793 (1997).
- <sup>23</sup> V.V. Moshchalkov, M. Baert, V.V. Metlushko, E. Rosseel, M.J. Van Bael, K. Temst, R. Jonckheere and Y. Bruynseraede, *Phys. Rev. B* **54**, 7385 (1996).
- <sup>24</sup> R. Benoist and W. Zwerger, *Z. Phys. B* **103**, 377 (1997).
- <sup>25</sup> D. Saint-James and P.-G. de Gennes, *Phys. Lett.* **7**, 306 (1963).
- <sup>26</sup> H.T. Jadallah, J. Rubinstein and P. Sternberg, *Phys. Rev. Lett.* **82**, 2935 (1999).
- <sup>27</sup> M. Tinkham, *Introduction to Superconductivity*, McGraw Hill, New York, 1975.
- <sup>28</sup> C. Strunk, V. Bruyndoncx, V.V. Moshchalkov, C. Van Haesendonck, Y. Bruynseraede and R. Jonckheere, *Phys. Rev. B* **54**, R12701 (1996).
- <sup>29</sup> C. Strunk, V. Bruyndoncx, C.-J. Chien, B. Burk, C. Van Haesendonck, V.V. Moshchalkov,

- Y. Bruynseraede and V. Chandrasekhar, Phys. Rev. B **57**, 10854 (1998) and references therein.
- <sup>30</sup> M. Park, M.S. Isaacson and J.M. Parpia, Phys. Rev. Lett. **75**, 3740 (1995).
- <sup>31</sup> C.S. Mkrtchyan and V.V. Shmidt, Sov. Phys. JETP **34**, 195 (1972).
- <sup>32</sup> V.M. Fomin, V.R. Misko, J.T. Devreese and V.V. Moshchalkov, Solid State Comm. **101**, 303 (1997).
- <sup>33</sup> V.M. Fomin, J.T. Devreese and V.V. Moshchalkov, Europhys. Lett. **42**, 553 (1998).
- <sup>34</sup> V.M. Fomin, J.T. Devreese and V.V. Moshchalkov, Europhys. Lett. **46**, 118 (1999).

## FIGURES

FIG. 1. AFM images of the three structures: (a) full, (b) 4-antidot, and (c) 2-antidot microsquares.

FIG. 2.  $T_c(H)$  phase boundaries for the (a) full, (b) 4-antidot, and (c) 2-antidot microsquares. For the full microsquare (a) we also present the calculated  $H_{c3}$  for an equivalent disk (Eq. (3)). The straight solid line is the calculated upper critical field  $H_{c2}$  (substitute  $n = 0$  in Eq. (3)). The parabola (dashed) indicates the low field  $T_c(H)$  behavior (Eq. (4)). The dashed line in (b) gives the parabolic background depression of  $T_c$  (Eq. (6)) for structures made of quasi-one-dimensional strips.

FIG. 3.  $T_c(\Phi)$  phase boundaries in reduced units of critical temperature and flux. For  $\Phi/\Phi_0 > 5$  the peaks in  $T_c(\Phi)$  appear at the same flux  $\Phi/\Phi_0$  in all the structures. The inset shows a comparison of the peak positions in  $T_c(\Phi)$  with the predictions for a mesoscopic disk. The scaling of the theoretical values (in flux units) gives the effective area of the microsquare.

FIG. 4. Low field part (single period) of the experimental phase boundary  $T_c(H)$  of the 4-antidot sample (where a parabolic background (Eq. (6)) has been subtracted) compared with the  $T_c(H)$  calculated from the dGA model for a  $2 \times 2$  cell network made of one-dimensional strips (see Refs.<sup>10,8</sup>), and using  $\xi(0)=92$  nm (dashed line), obtained for the full square, and  $\xi(0)=140$  nm (solid curve), estimated from the parabolic background (Eq. (6)) and an average strip width of  $0.4 \mu m$ .

FIG. 5. (a) Calculated phase boundaries (i.e., the  $H_{c3}(T)$  curves) for a circular antidot (Eq. (7)) and a dot (Eq. (2)) in normalized units of temperature and magnetic flux. Superconductivity will always nucleates initially near the dot/insulator boundary (the dot has the highest  $H_{c3}$ ). (b) Plot of the enhancement factor  $\eta$  (corresponding to  $H_{c3}/H_{c2}$ ) for the same structures.

FIG. 6. Calculation of the modulus of the superconducting order parameter  $|\Psi|$  for a disk, where  $R$  is the disk radius, and  $r$  the distance measured from the sample center to the sample boundary. The different curves are calculated for several values for  $\Phi/\Phi_0$  at the phase boundary  $H_{c3}(T)$ . The inset shows the normalized width of the superconducting edge state as a function of  $\Phi/\Phi_0$ .

TABLES

<b>Low H</b>	area ( $\mu\text{m}^2$ )	$T_c(0)$ (K)	$\mu_0 H_0$ (mT)	eff. area ( $\mu\text{m}^2$ )	$\xi(0)$ (nm)	$\ell$ (nm)	$\lambda(0)$ (nm)
<i>full square</i>	4.16	1.361	0.53	3.9	92	7	140
<i>4-antidot</i>	4.16	1.353	0.53	3.9	92	7	140
<i>2-antidot</i>	4.58	1.369	0.57	4.15	92	7	140

TABLE I. Values of several characteristic magnitudes for the three structures. The field corresponding to one flux quantum,  $\mu_0 H_0$ , and the effective areas are obtained by matching of the position of high field peaks to the theoretical location for a mesoscopic disk. The characteristic superconducting lengths for the full square are obtained from the low field behavior of  $T_c(\Phi)$  (Eq. (4)) and we assume the same values for the other structures.

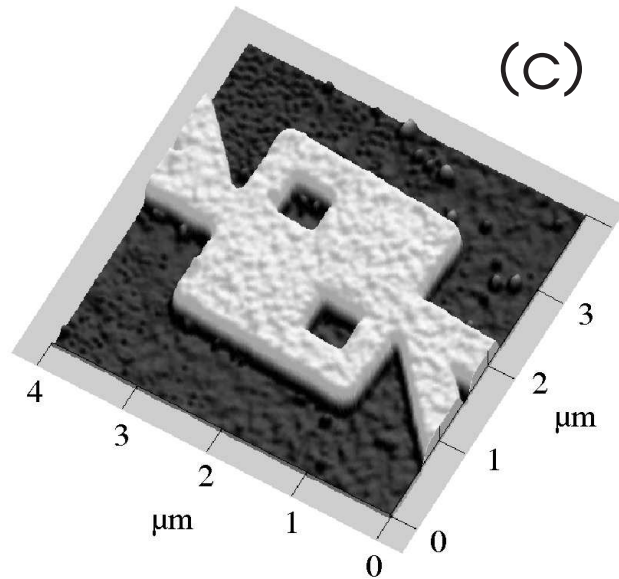
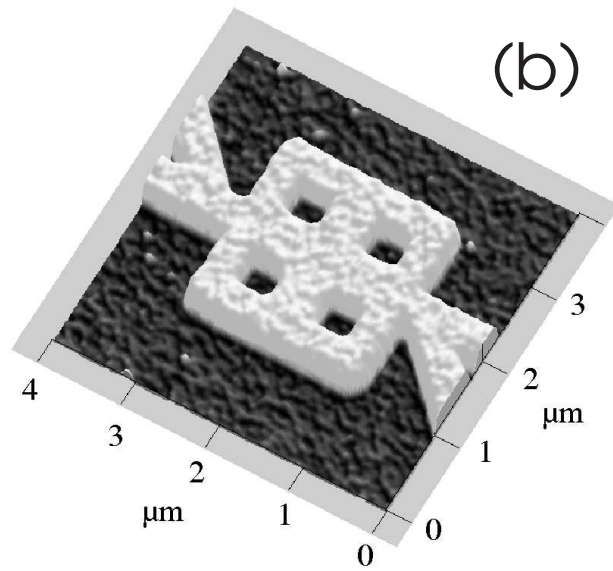
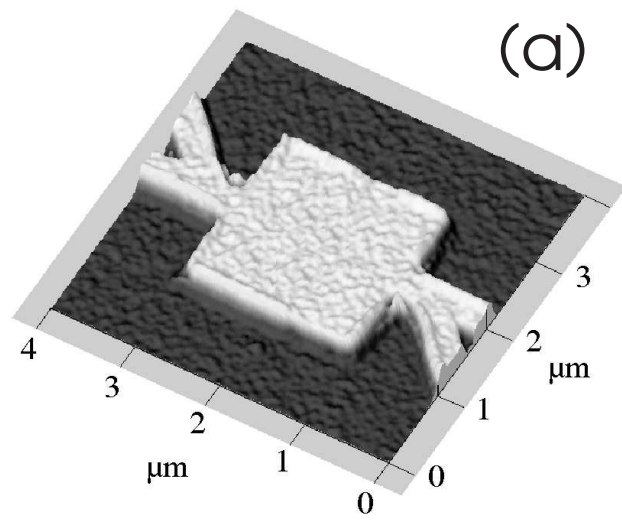


Fig. 1

Fig.2

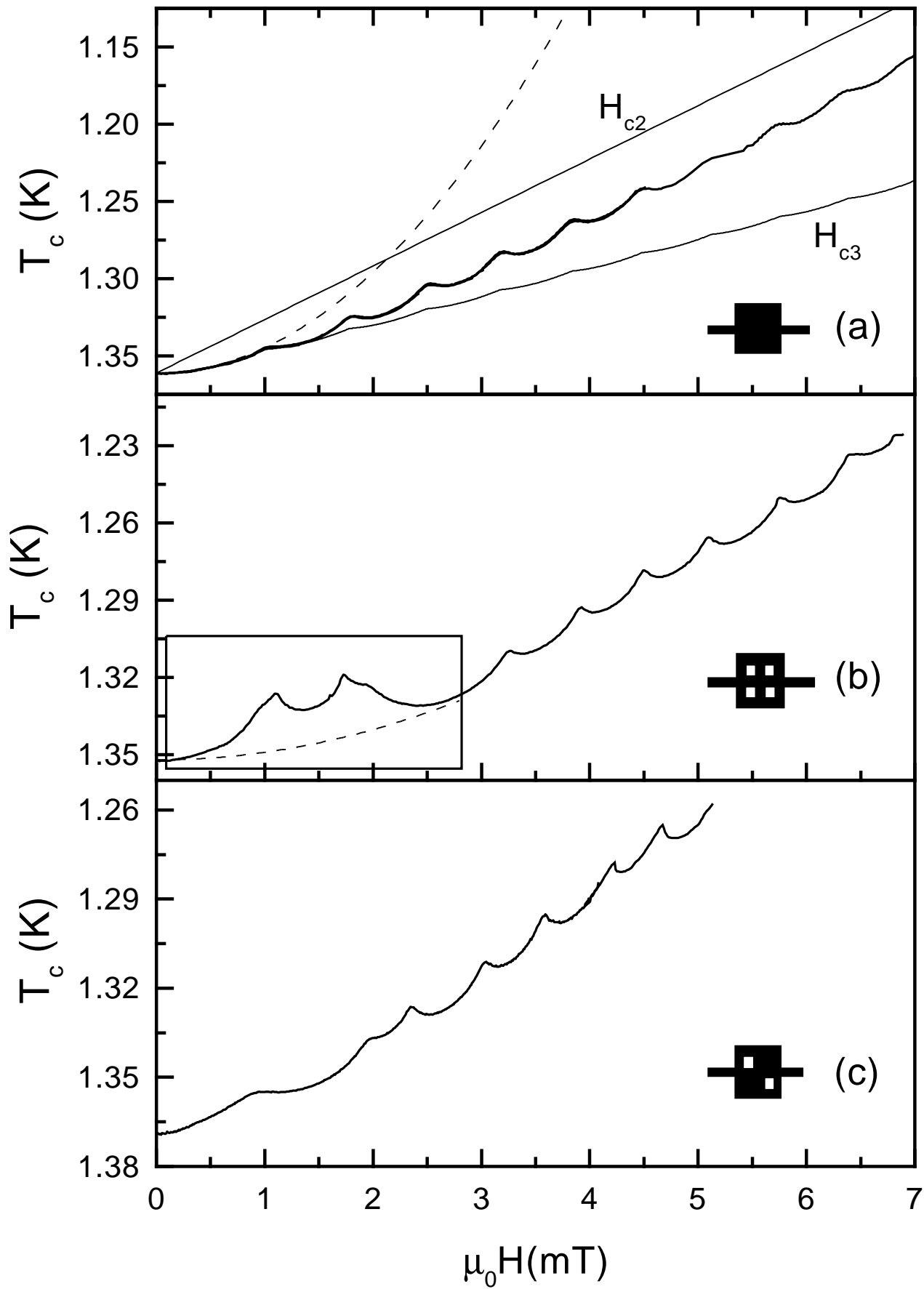




Fig.3

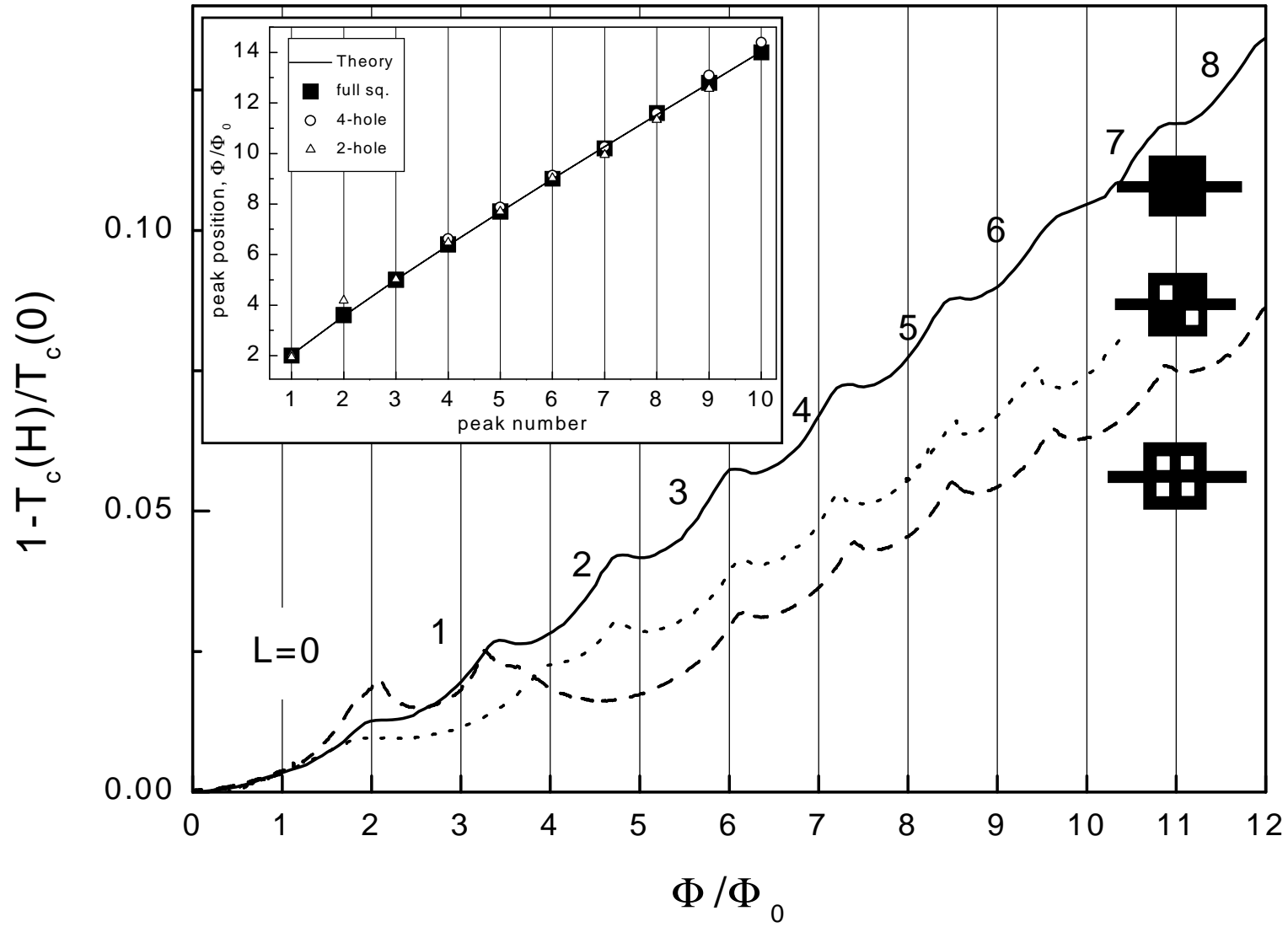


Fig.4

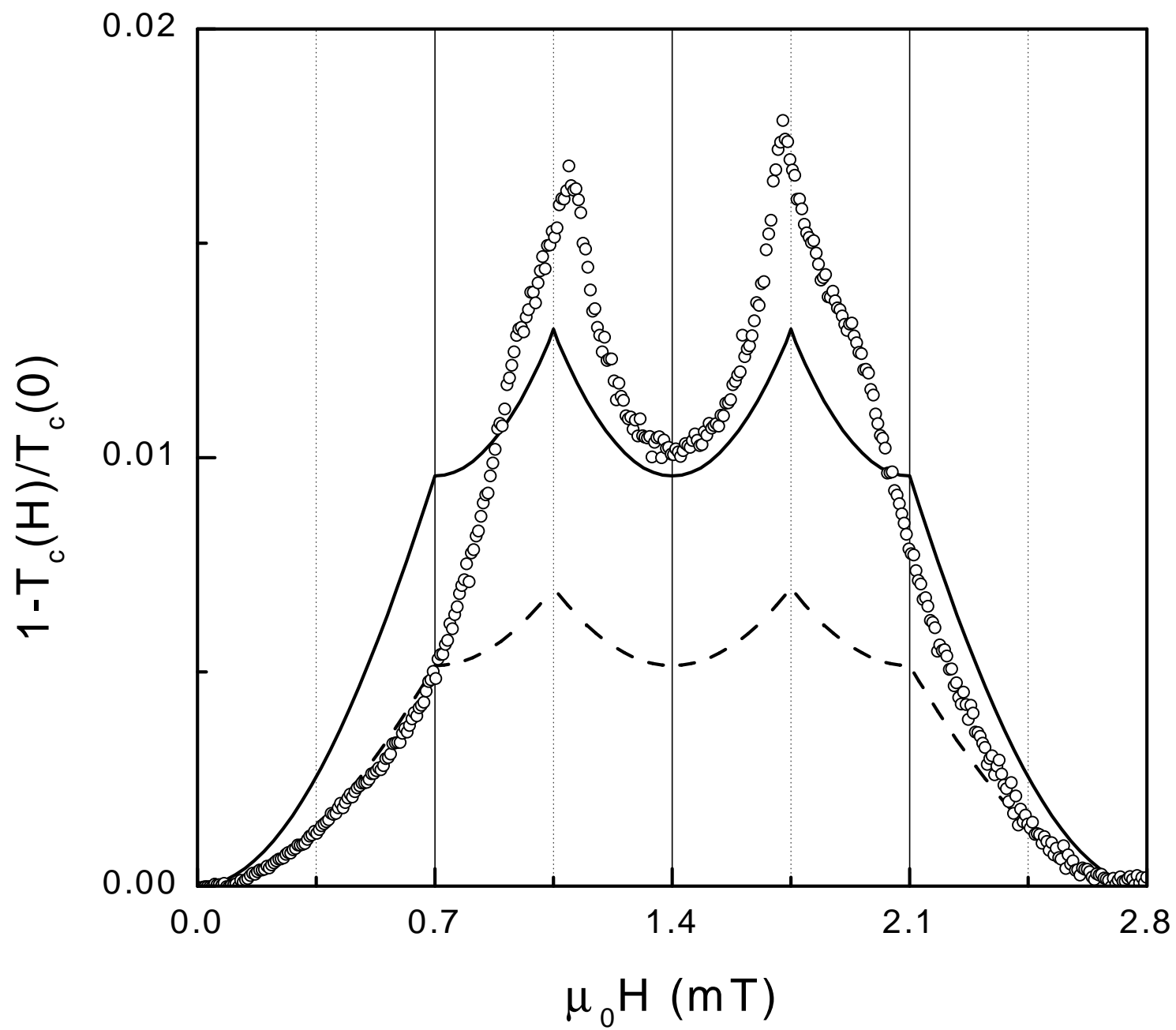


Fig.5

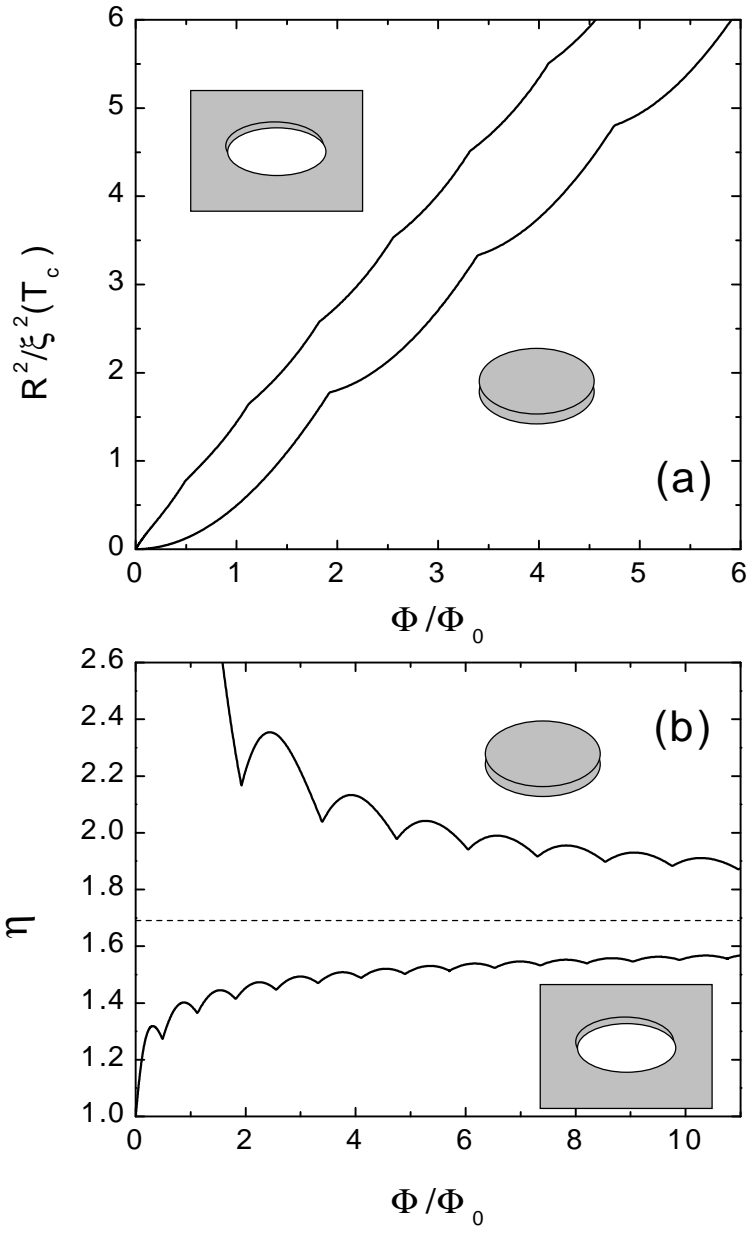


Fig.6

